

Monitoring fluid saturation in reservoirs using time-lapse full-waveform inversion

Amir Mardan^{1,2} | Bernard Giroux¹ | Gabriel Fabien-Ouellet³ | Mohammad Reza Saberi⁴

¹INRS-ETE, Québec, QC, Canada

²Geostack, Québec, QC, Canada

³Polytechnique Montréal, Montréal, Quebec, Canada

⁴GeoSoftware, Den Haag, The Netherlands

Correspondence

Amir Mardan, INRS-ETE, 490 Rue de la Couronne, and Geostack, 1st Avenue, Québec, QC, G1K 9A9, G1H 2W8, Canada.
Email: mardan.amir.h@gmail.com

Abstract

Monitoring the rock physics properties of the subsurface is of great importance for reservoir management. For either oil and gas applications or CO₂ storage, seismic data are a valuable source of information for tracking changes in elastic properties which can be related to fluids saturation and pressure changes within the reservoir. Changes in elastic properties can be estimated with time-lapse full-waveform inversion. Monitoring rock physics properties, such as saturation, with time-lapse full-waveform inversion is usually a two-step process: first, elastic properties are estimated with full-waveform inversion, then the rock physics properties are estimated with rock physics inversion. However, multiparameter time-lapse full-waveform inversion is prone to crosstalk between parameter classes across different vintages. This leads to leakage from one parameter class to another, which, in turn, can introduce large errors in the estimated rock physics parameters. To avoid inaccuracies caused by crosstalk and the two-step inversion strategy, we reformulate time-lapse full-waveform inversion to estimate directly the changes in the rock physics properties. Using Gassmann's model, we adopt a new parameterization containing porosity, clay content and water saturation. In the context of reservoir monitoring, changes are assumed to be induced by fluid substitution only. The porosity and clay content can thus be kept constant during time-lapse inversion. We compare this parameterization with the usual density–velocity parameterization for different benchmark models. Results indicate that the proposed parameterization eliminates crosstalk between parameters of different vintages, leading to a more accurate estimation of saturation changes. We also show that using the parameterization based on porosity, clay content and water saturation, the elastic changes can be monitored more accurately.

KEY WORDS

elastics, full waveform, inversion, monitoring, time lapse

INTRODUCTION

Either for oil and gas applications or CO₂ sequestration, the ability to monitor reservoirs is highly important as it allows for

safe and profitable operations. Time-lapse seismic monitoring is a powerful tool that allows to investigate large-scale changes in a reservoir (Lumley, 2001; Landrø et al., 2003; Dupuy et al., 2016; Maharramov et al., 2016; Fabien-Ouellet et al.,

This is an open access article under the terms of the Creative Commons Attribution License, which permits use, distribution and reproduction in any medium, provided the original work is properly cited.

© 2023 The Authors. *Geophysical Prospecting* published by John Wiley & Sons Ltd on behalf of European Association of Geoscientists & Engineers.



2017; Lang & Grana, 2019; Zhou & Lumley, 2021; Mardan et al., 2022b, 2022d, 2022a). Seismic monitoring is sensitive to changes in elastic parameters, which can be related to reservoir parameters, such as saturation, through a rock physics model.

Numerous studies have been conducted to monitor saturation changes in reservoirs. Landrø et al. (2003) used PP and PS seismic data to better estimate the time-lapse changes. Buland and Ouair (2006) proposed a Bayesian time-lapse inversion method and applied it to monitor the Norne Field offshore Norway with seismic data acquired from 2001 to 2003. Vedanti and Sen (2009) used prestack seismic data inversion to monitor the in situ combustion in the Balol oil field. Lang and Grana (2019) studied the potential of the Johansen field in Norway by simulating CO₂ injection for 10 years and monitoring the reservoir. All of these studies are based on linearized amplitude variation with offset (AVO) and the convolutional model whose accuracy decreases by increasing the incidence angle (Mallick, 2007). Although AVO has been very successful and is commonly used in industry, it has some other limitations. AVO inversion only uses the amplitude of the reflected waves, while for better imaging all types of waves should be involved during the inversion (Virieux et al., 2017). In addition, AVO relies on the assumption that reflectors are flat, which is a restrictive hypothesis in many cases (Queißer & Singh, 2013). Last but not least, AVO suffers from the uncertainties in data preprocessing such as velocity model errors (Naeini et al., 2017; Hu et al., 2021). These assumptions and the incomplete use of waveforms can lead to suboptimal use of the resources invested in monitoring.

A variety of studies have used time-lapse full-waveform inversion (TL-FWI) to monitor reservoirs. For example, Watanabe et al. (2005) used time-lapse crosswell seismic data to monitor the changes during a gas hydrate thermal production test at the Mallik site. Raknes et al. (2013) monitored the leakage of one producing well over a field in the North Sea by studying the seismic data of two vintages with 2 years time difference. Hicks et al. (2016) and Lescoffit et al. (2016) showed the interest in TL-FWI when studying seismic data and changes in P-wave velocity (V_P) at the Grane field due to gas–oil replacement. Maharramov et al. (2016) showed the potential of TL-FWI to image the changes in the Genesis field in the Green Canyon area of the central Gulf of Mexico. In these studies, TL-FWI is carried out to map the acoustic changes in the subsurface using a monoparameter acoustic formulation (analysing only V_P). To obtain the changes in terms of rock physics properties, full-waveform inversion (FWI) is employed to estimate V_P and in the next step, the estimated V_P is inverted using rock physics inversion. For example, this two-step procedure has been used to estimate the changes in the saturation of CO₂ at the Sleipner

field in the North Sea (Queißer & Singh, 2013; Dupuy et al., 2016; Dupuy et al., 2016; Yan et al., 2019; Dupuy et al., 2021; Romdhane et al., 2022).

To approach the true properties of the subsurface, an elastic formulation is preferred over acoustic as it allows taking into account the different seismic phases in the measured data. An elastic medium requires multiparameter TL-FWI. In this case, model parameters can have coupled effects on the seismic data, which are referred to as crosstalk between parameters (Operto et al., 2013; Yang et al., 2018). Ma et al. (2016) studied the Marmousi model for multiparameter acoustic TL-FWI and showed that the crosstalk problem is more severe in TL-FWI. Although Ma et al. (2016) recovered good images of the subsurface using FWI, the estimated *time-lapse* images were inaccurate due to the crosstalk problem (figs. 2 and 3 of Ma et al., 2016). This problem can be alleviated by using different parameterizations (Tarantola, 1986; Operto et al., 2013; Ma et al., 2016; Hu et al., 2021). A comprehensive discussion is provided by Pan et al. (2019) where the authors analysed the efficiency of different parameterizations such as velocity–density (P-wave velocity, S-wave velocity and density), modulus–density (bulk modulus, shear modulus and density), impedance–density (P-wave impedance, S-wave impedance and density), velocity–impedance-I (P-wave velocity, S-wave velocity and P-wave impedance) and velocity–impedance-II (P-wave velocity, S-wave velocity and S-wave impedance) for performing elastic FWI.

The goal of this study is to recover the changes in water saturation (S_w) by considering an elastic earth. To minimize the effects of crosstalk that can occur due to the time-lapse nature of the problem, the TL-FWI is formulated in terms of porosity (ϕ), clay content (C) and water saturation (PCS), as proposed by Hu et al. (2021) in the context of FWI. This parameterization is chosen to facilitate the time-lapse inversion as we can assume that porosity and clay content are constant with time in the reservoir. To perform this technique, a connection between the elastic and rock-physical properties is required. In this work, we use Gassmann's equation for this purpose. Using the PCS parameterization, we combine the rock physics inversion and FWI in a single inversion scheme. In this way, saturation can be directly inverted from the raw seismic data (shot gather). By performing TL-FWI with the PCS parameterization, we can also easily obtain the time-lapse images of elastic properties using the underlying rock physics model.

This paper is organized by first presenting FWI and the required formulation to include Gassmann's model for estimating the porosity, clay content and water saturation. This section is followed by a brief discussion on TL-FWI. Then, we study and discuss the efficiency of this method by using numerical models.

THEORY

Full-waveform inversion

Full-waveform inversion (FWI) is a local optimization process that minimizes residuals between the observed and estimated wavefields at the receivers locations for different source positions (Virieux & Operto, 2009). The objective function can be written as

$$\chi(\mathbf{m}) = \frac{1}{2} \|\mathbf{W}_d(\mathbf{R}\mathbf{u}(\mathbf{m}) - \mathbf{d})\|_2^2 + \chi_{REG}, \quad (1)$$

where \mathbf{R} maps the wavefield (\mathbf{u}) to the receivers locations. Vectors \mathbf{m} and \mathbf{d} are the model parameter and observed data, respectively. \mathbf{W}_d is a weighting operator on the data misfit and χ_{REG} is a regularization term. FWI is highly ill-posed, where an infinite number of models match the data. A variety of regularization methods such as the Tikhonov, total variation, prior information and parameter-relation techniques have been proposed to condition the FWI problem and reduce the ill-posedness (Virieux & Operto, 2009; Asnaashari et al., 2015). In this study, we use the Tikhonov regularization. This regularization method is presented in the Appendix in addition to total variation, prior information and parameters-relation techniques. In Equation (1), the wavefield is the solution of a partial differential equation (PDE) which is discretized to perform the forward modelling. For the two-dimensional isotropic elastic case in the time domain, this PDE can be written as

$$\begin{cases} \rho \dot{v}_x = \partial_x \tau_{xx} + \partial_z \tau_{xz}, \\ \rho \dot{v}_z = \partial_z \tau_{zz} + \partial_x \tau_{xz}, \\ \dot{\tau}_{xx} = (\lambda + 2G)\partial_x v_x + \lambda \partial_z v_z + s, \\ \dot{\tau}_{zz} = \lambda \partial_x v_x + (\lambda + 2G)\partial_z v_z + s, \\ \dot{\tau}_{xz} = G(\partial_z v_x + \partial_x v_z), \end{cases} \quad (2)$$

where λ and G denote Lamé's parameter and where ρ and s are density and the source function. In Equation (2), the particle velocities in x - and z -directions (v_x and v_z) as well as (τ_{xx} and τ_{zz}) and shear stresses (τ_{xz}) constitute vector \mathbf{u} . Spatial partial derivative operators are indicated by ∂_x and ∂_z for x - and z -directions, and the temporal differentiation is denoted by overhead dot ($\dot{\square}$).

In the case of Equation (2), the vector of model parameter, \mathbf{m} in Equation (1), is

$$\mathbf{m} = [\lambda, G, \rho]^T, \quad (3)$$

where T is the transpose operator. Although the forward modelling is performed using Lamé parameters and density, FWI can be performed using different parameterizations. For example, the velocity–density (DV) parameterization is

a common formulation. Switching between parameters can be carried out using the chain rule, as shown at the end of this section.

Optimization

To minimize the cost function (Equation 1), a variety of optimization algorithms such as steepest-descent, conjugate-gradient, ℓ -BFGS (Limited-memory Broyden-Fletcher-Goldfarb-Shanno) and Newton algorithms can be employed (Virieux & Operto, 2009). These algorithms minimize the cost function in the vicinity of a starting model, \mathbf{m}_0 , as

$$\mathbf{m} = \mathbf{m}_0 + \alpha \Delta \mathbf{m}, \quad (4)$$

where α is step size and the search direction, $\Delta \mathbf{m}$, for gradient descent is

$$\Delta \mathbf{m} = - \begin{bmatrix} \nabla_{\mathbf{m}^{(1)}} \chi \\ \nabla_{\mathbf{m}^{(2)}} \chi \\ \nabla_{\mathbf{m}^{(3)}} \chi \end{bmatrix}, \quad (5)$$

where $\nabla_{\mathbf{m}^{(n)}} \chi$ is the gradient of the cost function with respect to model parameter $\mathbf{m}^{(n)}$.

One of the most problematic challenges of multiparameter FWI is crosstalk between parameters. Crosstalk is due to the fact that different parameters can have a coupled effect on the seismic wavefield and different combinations of changes in these parameters can cause similar seismic response (Operto et al., 2013; Yang et al., 2018). To address this problem, different strategies have been deployed (Fabien-Ouellet et al., 2017; Keating & Innanen, 2019; Lavoué et al., 2014; Métivier et al., 2013; Operto et al., 2013). Operto et al. (2013) listed four main strategies: the choice of appropriate parameterization, the use of the Hessian as it can measure the level of coupling between parameters, a data-driven strategy, that is, using multi-components data and a sequential inversion where the dominant parameters are estimated before the secondary parameters. To further reduce the crosstalk problem, it is also proposed to scale the gradient (Kamei & Pratt, 2013; Lavoué et al., 2014). Hence, Equation (5) can be rewritten as

$$\Delta \mathbf{m} = - \begin{bmatrix} \nabla_{\mathbf{m}^{(1)}} \chi \\ \xi \nabla_{\mathbf{m}^{(2)}} \chi \\ \beta \nabla_{\mathbf{m}^{(3)}} \chi \end{bmatrix}, \quad (6)$$

where ξ and β scale the gradient of different parameter classes.

By using a quasi-Newton method, ℓ -BFGS, we consider an approximation of the Hessian into the solution (Nocedal & Wright, 2006) which helps reducing crosstalk. However, the most important point of this study is the chosen



parameterization. Considering the fact that the time-lapse changes in P-wave velocity due to fluid substitution (more affected than S-wave velocity and density) are approximately 10% of the baseline model (Zhou & Lumley, 2021), the challenges of FWI are more pronounced in time-lapse studies than in conventional FWI. Ma et al. (2016) studied the possibility of deploying time-lapse full-waveform inversion (TL-FWI) for multiparameter acoustic studies. Although they estimate the model parameters very well, crosstalk prevents from obtaining an acceptable time-lapse image of the subsurface for any of two time-variable parameters. Thereby, an efficient parameterization is required to minimize the crosstalk in multiparameter TL-FWI. Inspired by Hu et al. (2021), we study the feasibility of performing TL-FWI using the PCS parameterization. Recalling that the porosity and clay content can be reasonably considered constant with time, water saturation is the only time-variable parameter.

In the next section, we provide the required equations to adapt the FWI problem to estimate the PCS parameters using Gassmann's equation. In this case, the vector of the model parameter can be written as

$$\mathbf{m} = [\phi, C, S_w]^T. \quad (7)$$

Using the aforementioned assumption that porosity and clay content remain constant over time for reservoirs, the changes in water saturation can be the only parameter to be sought in the time-lapse inversion.

It is worth recalling that the chain rule is used to change the parameters for inversion. As an example, \mathbf{q} parameterization, $\mathbf{q} = [q_1, q_2, q_3]^T$, can be changed to a new parameterization, $\mathbf{p} = [p_1, p_2, p_3]^T$, as

$$\frac{\partial \chi}{\partial q_i} = \frac{\partial \chi}{\partial p_1} \frac{\partial p_1}{\partial q_i} + \frac{\partial \chi}{\partial p_2} \frac{\partial p_2}{\partial q_i} + \frac{\partial \chi}{\partial p_3} \frac{\partial p_3}{\partial q_i}, \quad (8)$$

for $i \in (1, 2, 3)$. FWI can be performed in any parameterization while the forward modelling is implemented using Equation (2).

This study is carried out using PyFWI (Mardan et al., 2023a), which is an open-source package that implements FWI in terms of DV parameterization. In the next section, we present the methodology to transfer the earth model from PCS parameterization to DV parameterization for forward modelling. In the Appendix, we present the required equations to obtain the gradient of the cost function in terms of PCS parameterization for performing the inversion.

Porous media homogenization

To perform TL-FWI with a rock physics parameterization, a rock physics model is needed to map the rock physics prop-

erties to the elastic properties. Although there are numerous empirical rock physics models that satisfy this requirement, we employ Gassmann's equation (Gassmann, 1951) which is valid for most of consolidated rocks (Dupuy et al., 2016). Gassmann's relation is used to compute the variation of bulk modulus during the fluid substitution. In practice, Gassmann's model requires some information on the fluid and mineral properties. In the context of TL-FWI, this information should be available as time-lapse FWI is usually performed in well-studied fields.

The effective properties of the fluid (bulk modulus, K , and density) can be calculated using weighted arithmetic averages (Voigt, 1889),

$$\begin{aligned} K_f &= S_w K_w + (1 - S_w) K_h, \\ \rho_f &= S_w \rho_w + (1 - S_w) \rho_h, \end{aligned} \quad (9)$$

where the subscripts f , w and h , respectively, denote the effective property of the fluid, water and hydrocarbon.

The density of the solid frame of rock can be calculated using a weighted average of the density of the grains as

$$\rho_s = C \rho_c + (1 - C) \rho_q, \quad (10)$$

where subscripts s , c and q denote solid medium, clay and quartz, respectively. The bulk and shear moduli of the solid can be estimated using the Voigt–Reuss–Hill method

$$\begin{aligned} K_s &= \frac{1}{2} \left[(C K_c + (1 - C) K_q) \right. \\ &\quad \left. + \left(\frac{1}{C/K_c + (1 - C)/K_q} \right) \right], \\ G_s &= \frac{1}{2} \left[(C G_c + (1 - C) G_q) \right. \\ &\quad \left. + \left(\frac{1}{C/G_c + (1 - C)/G_q} \right) \right]. \end{aligned} \quad (11)$$

The effective dry moduli of the rock, K_D and G_D can be computed using various effective medium theories (Berryman, 1995; Mavko et al., 2020). Following Pride (2005), we estimate the dry moduli with

$$\begin{aligned} K_D &= K_s \frac{1 - \phi}{1 + cs\phi}, \\ G_D &= G_s \frac{1 - \phi}{1 + \frac{3}{2}cs\phi}, \end{aligned} \quad (12)$$

where cs is the general consolidation parameter which defines the degree of consolidation among grains. This parameter can be considered as a free parameter in predicting velocities (Lee, 2005). For further studies about cs , readers are referred to

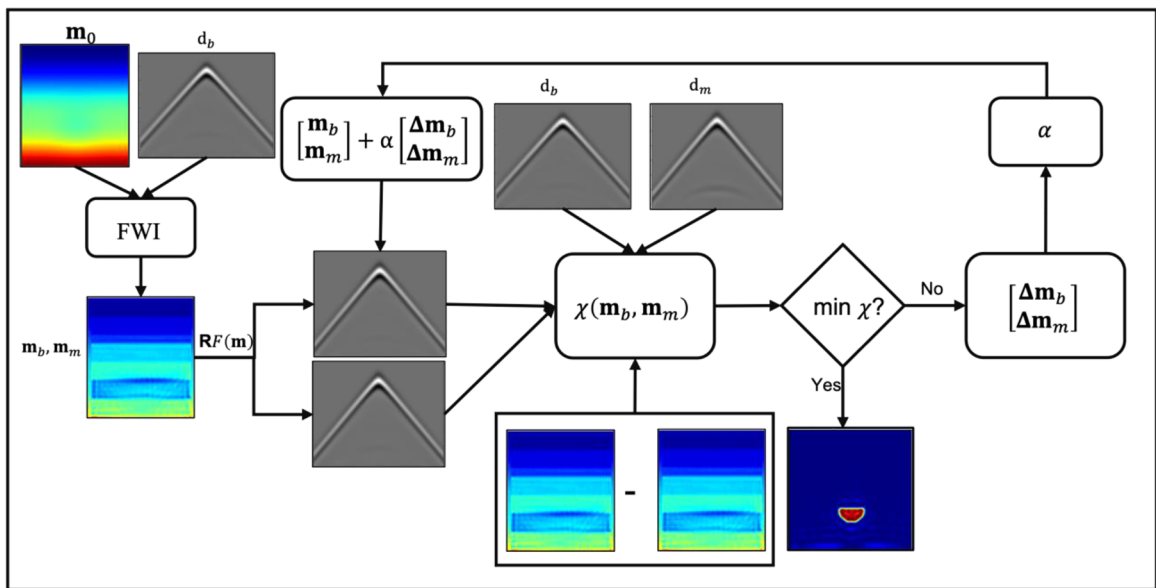


FIGURE 1 Flowchart of simultaneous TL-FWI. After performing FWI on baseline data, a joint time-lapse FWI inverts baseline and monitor data where the inversion process is regularized by the difference between estimated baseline and monitor models.

TABLE 1 Elastic properties in this study for minerals and fluids where c_s is set to 20 (Dupuy et al., 2016; Hu et al., 2021).

| | Bulk modulus (GPa) | Shear modulus (GPa) | Density (g/cm ³) |
|--------|--------------------|---------------------|------------------------------|
| Quartz | 37.00 | 44.00 | 2.65 |
| Clay | 21.00 | 10.0 | 2.55 |
| Water | 2.25 | 0.00 | 1.00 |
| Gas | 0.04 | 0.00 | 0.10 |

Lee (2005) where the author discusses the importance of this parameter and how it can be calculated.

Finally, the effective properties of the porous medium are calculated with the following expressions (Gassmann, 1951; Voigt, 1889):

$$K = \frac{\phi K_D + (1 - (1 + \phi)K_D/K_s)K_f}{\phi(1 + \Delta)}, \quad (13)$$

$$G = G_D,$$

$$\rho = (1 - \phi)\rho_s + \phi\rho_f,$$

where

$$\Delta = \frac{1 - \phi}{\phi} \frac{K_f}{K_s} \left(1 - \frac{K_D}{(1 - \phi)K_s} \right) = \frac{1 - \phi}{\phi} \frac{K_f}{K_s} \left(1 - \frac{1}{1 + c_s \phi} \right). \quad (14)$$

The elastic properties can be calculated using Equation (13) as

$$V_P = \sqrt{\frac{K + \frac{4}{3}G}{\rho}}, \quad (15)$$

$$V_S = \sqrt{\frac{G}{\rho}},$$

$$\rho = \rho.$$

For a detailed discussion on Gassmann's model and the provenance of Equations (9)–(15), see Dupuy et al. (2016).

Time-lapse full-waveform inversion

Time-lapse FWI can be performed by considering different combinations of FWI runs. These combinations can be performed sequentially such as for the cases of the cascaded, cross-updating and weighted-average methods (Watanabe et al., 2005; Maharramov et al., 2016; Mardan et al., 2022c, 2023b) or in parallel as in the case of the independent and central-difference methods (Plessix et al., 2010; Zhou & Lumley, 2021). In addition to these methods, Maharramov et al. (2016) proposed a joint inversion of seismic data from different vintages by introducing the cost function as

$$\chi_{tl}(\mathbf{m}_b, \mathbf{m}_m) = \|\mathbf{R}\mathbf{u}(\mathbf{m}_b) - \mathbf{d}_b\|_2^2 + \|\mathbf{R}\mathbf{u}(\mathbf{m}_m) - \mathbf{d}_m\|_2^2 + \delta \|\mathbf{m}_m - \mathbf{m}_b\|_2^2 \quad (16)$$

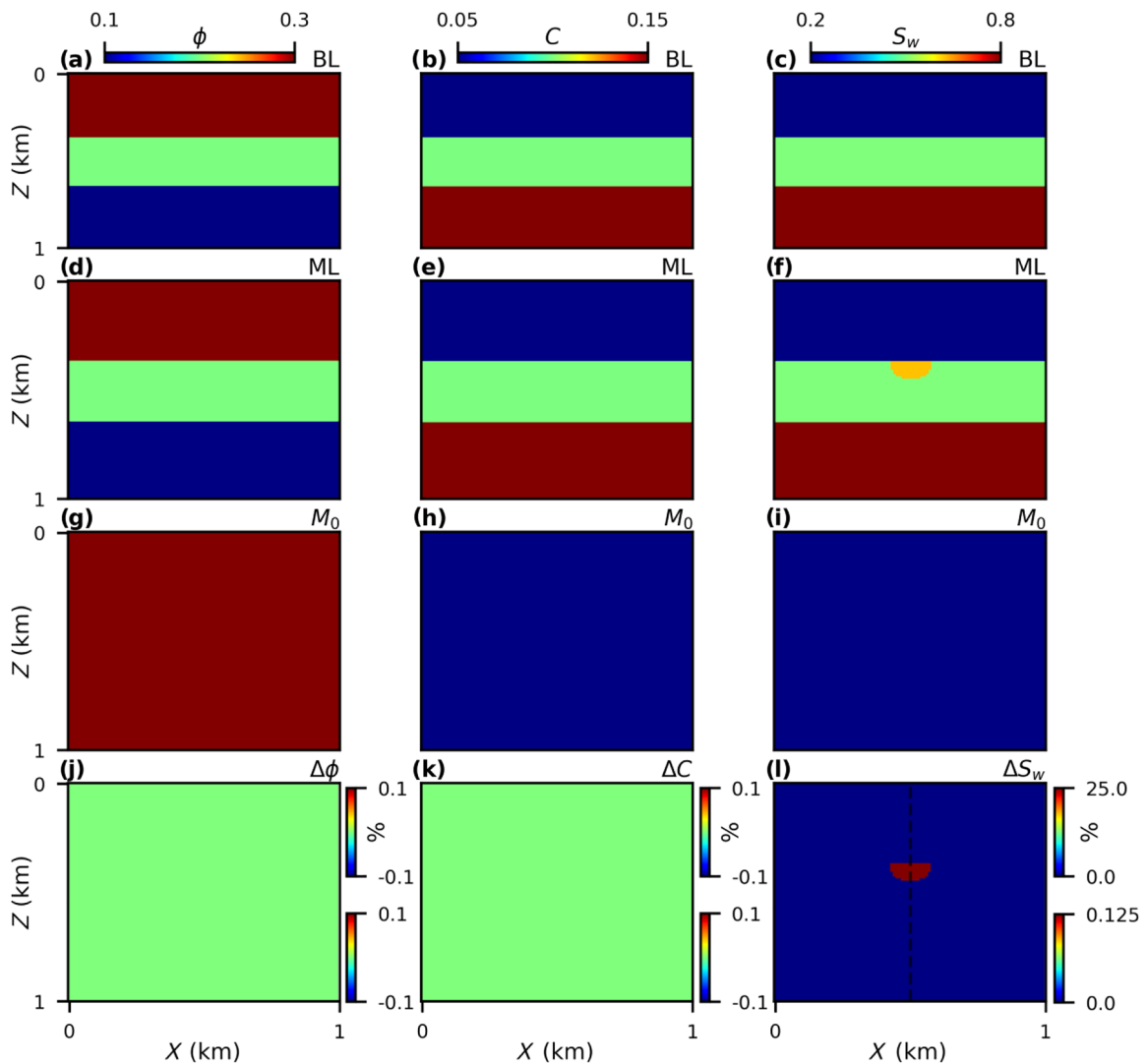


FIGURE 2 Rock physics properties of the layered model. (a)–(c) True baseline (BL), (d)–(f) true monitor (ML), and (g)–(i) initial models. (j)–(l) Time-lapse changes between porosity (a and d), clay content (b and e) and water saturation (c and f). The time-lapse model is presented with two color scales which show the changes in the value and percentage. The dashed line in (l) is used for the one-dimensional profile in Figures 5 and 8.

where subscripts b and m denote baseline and monitor models. The difference between the estimated baseline and monitor models is used as a regularization term and the weight of this term in the cost function is controlled by parameter δ which is constant during the inversion. This parameter, δ , can vary for different surveys and should be picked by trial and error. More details on this parameter can be found in Maharramov et al. (2016). The flowchart of this method (hereafter called simultaneous TL-FWI) is presented in Figure 1. Simultaneous TL-FWI gets an initial model and observed seismic data from two vintages. In the first step, the baseline data are inverted and the estimated baseline is used as the initial model for time-lapse FWI. TL-FWI minimizes the residuals between the estimated and observed data from the baseline and monitor models regularized by the difference between the estimated models.

Simultaneous TL-FWI is one of the most accurate strategies for time-lapse studies (Mardan et al., 2023b). Incorporating a regularization term for minimizing the difference between two estimates (baseline and monitor models) helps this method to produce less artefacts.

The methodology we propose is as follows. We first estimate the baseline model, using the standard FWI in the PCS parameterization. Then, we perform a single-parameter inversion of S_w by jointly inverting the baseline and monitor data (Equation 16). We justify the last step by making the hypothesis that porosity and clay content remains constant after fluid injection. In the case of inversion with the DV parameterization, the TL-FWI is a multiparameter problem. Furthermore, it requires the additional step of inverting the elastic properties to obtain S_w . In this work, we use ℓ -BFGS to do so, which minimizes the following cost

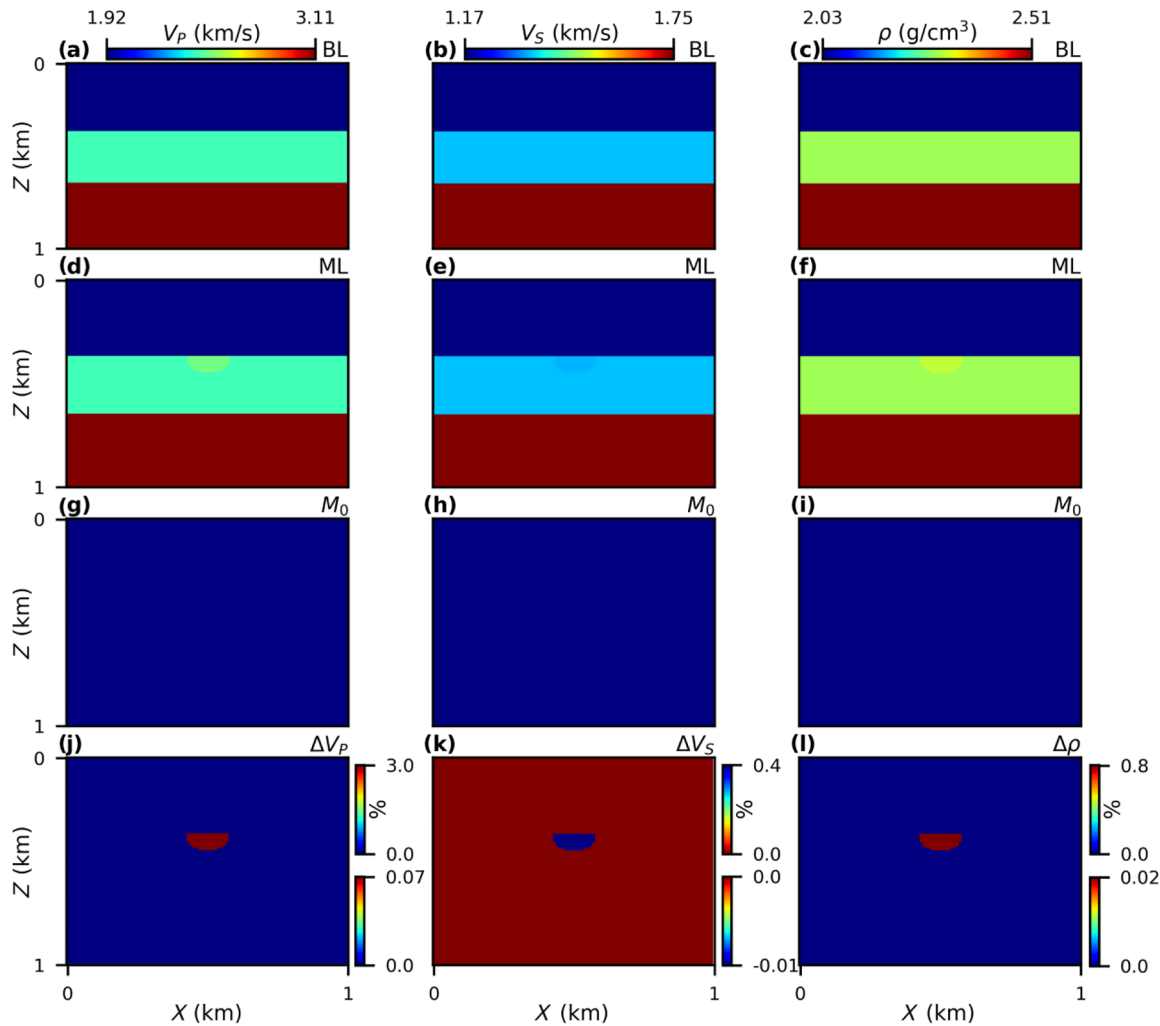


FIGURE 3 Elastic properties of the layered model. (a)–(c) True baseline (BL), (d)–(f) true monitor (ML), and (g)–(i) initial models. (j)–(l) Time-lapse changes between V_P (a and d), V_S (b and e) and ρ (c and f). The time-lapse model is presented with two color scales which show the changes in the value and percentage.

function:

$$\chi_{rp} = \frac{1}{2} \| F(\phi, C, S_w) - \mathbf{m}_{DV} \|^2, \quad (17)$$

where F is a function that calculates V_P , V_S and ρ based on Equations (9)–(15) and \mathbf{m}_{DV} is a vector of estimated elastic properties using the DV parameterization.

NUMERICAL ANALYSIS

In this section, we assess the feasibility of the proposed strategy with two synthetic models. For both analyses, full-waveform inversion (FWI) is performed to estimate all model properties (elastic or rock physics properties) simultaneously. In this regard, the multi-scale strategy (Bunks et al., 1995) is employed to avoid cycle skipping. We filter the observed and

estimated data using a lowpass Butterworth filter with cut-off frequencies of 10, 20, 25, 35, 40 and 55 Hz. The source for forward modelling is a Ricker wavelet with a central frequency of 30 Hz. Perfectly matched layers (PML) are used at the boundaries of the models to minimize waves reflected from the boundaries (Berenger, 1994). We use the Tikhonov regularization (Equation A.1) in the x -direction ($\mathbf{B}_z = 0$) to decrease the ill-posedness of the FWI problem and make the estimated models smoother in the x -direction.

For numerical studies, we use two synthetic models. For the first experiment, a simple layered model is used. Then, time-lapse full-waveform inversion (TL-FWI) is performed using the Marmousi model, which is a more realistic case. During the inversion, the gradient is scaled using Equation (6). The scaling weights ξ and β are obtained by trial and error, by performing FWI runs on the simple layered model. Then we use the same weights for the Marmousi model. The rock-physical properties used in this study are shown in Table 1.

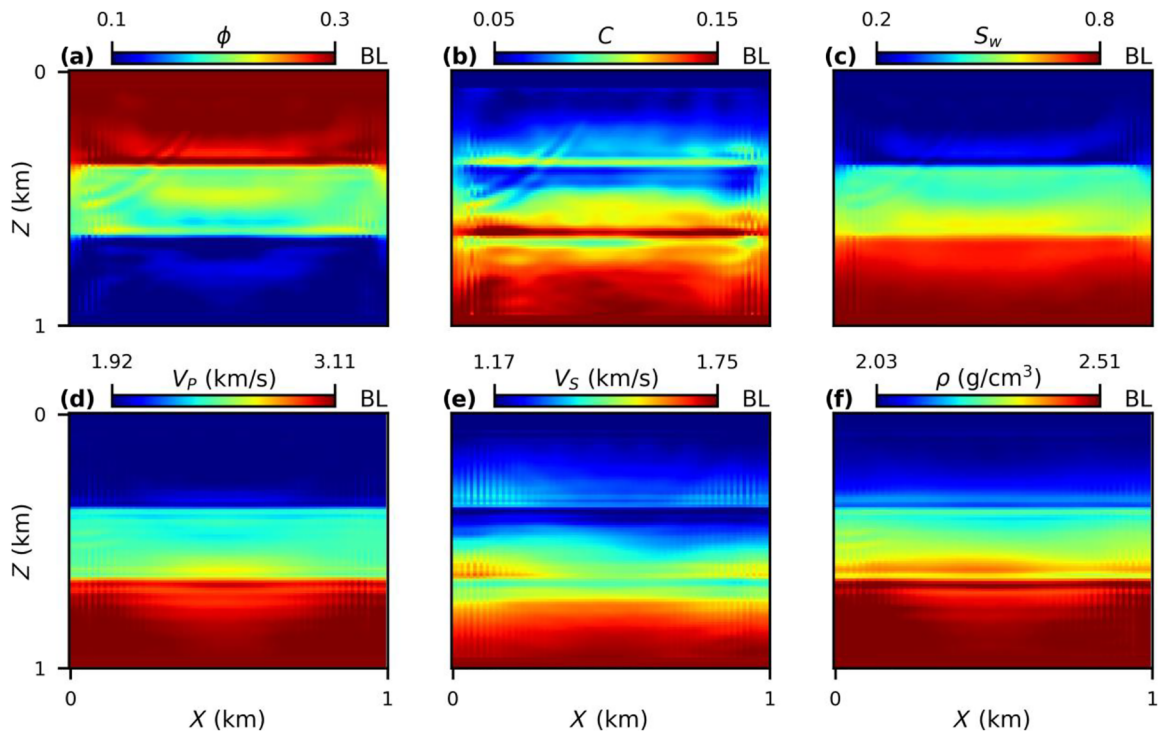


FIGURE 4 The estimated baseline model (BL) in terms of (a) porosity, (b) clay content, (c) water saturation, (d) P-wave velocity, (e) S-wave velocity and (f) density estimated using the PCS parameterization.

Layered model

To investigate the performance of the methodology, a simple model with three flat reflectors is first used (Figure 2). Figure 2a–c shows the true models for porosity, clay content and water saturation for the baseline, and Figure 2d–f shows the true monitor model. The initial model of the inversion is shown in Figure 2g–i. Finally, the true time-lapse model is shown in Figure 2j–l. The elastic properties of this model are shown in Figure 3. Comparing Figures 2j–l with Figure 3j–l shows that with a 25% increment of water saturation, P-wave velocity and density increase by 3% and 0.8%, respectively, while the S-wave velocity decreases by 0.4%.

To perform this study, seven isotropic sources are used on the surface for forward modelling. Receivers are located on the surface and in two imaginary wells on both sides of the model. Noise-free pressure data are inverted to recover the time-lapse anomaly. The rock physics properties estimated by using Gassmann's equation are presented in Figure 4a–c. The parameters in this model are used to obtain an indirect estimate of P- and S-wave velocities as well as density, as shown in Figure 4d,f. A one-dimensional (1D) plot obtained at $X = 0.5$ km (dashed line in Figure 2l) is also shown in Figure 5 for both rock physics properties (Figure 5a–c) and elastic properties (Figure 5d–f).

Results of the first step obtained with this simple synthetic model show that FWI and the proposed formulation

have the potential to recover the rock physics properties. However, reconstructing the clay content seems problematic, and the interfaces in this parameter are not recovered sharply (Figures 4b and 5b). Although Hu and Innanen (2021) showed that the C model can be estimated better by considering a parameter-relation regularization, this type of regularization is not taken into account in this study. The parameter-relation regularization allows us to regularize the inversion based on the relation between two parameters in the field. So, in general, we can expect that the parameter-relation and prior-model regularization (Asnaashari et al., 2013) should improve the accuracy of the estimated clay content. These two regularization methods are provided in the Appendix A for interested readers.

After estimating the baseline model (Figure 4), TL-FWI can be performed using Equation (16). We first compare the efficiency of the velocity–density (DV) and PCS parameterization to monitor the rock physics properties. Using the DV parameterization, changes in terms of the rock physics properties are estimated in two steps. We first estimate the elastic properties of the baseline and the monitor models using Equation (16). In the second step, Equation (17) is employed to estimate the rock physics properties of the baseline and the monitor models and differences, which are presented in Figure 6a–c. This is a naive method to perform multiparameter TL-FWI and leads to an overestimation of porosity and inaccurate time-lapse estimate. We cannot get an

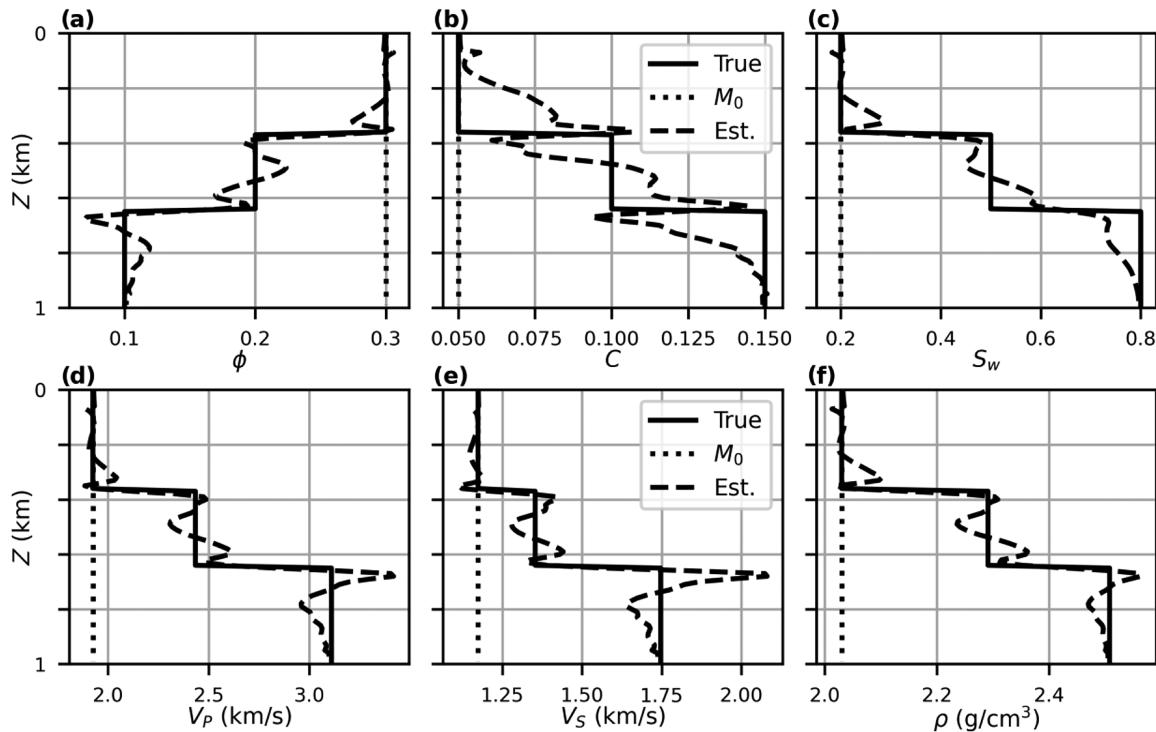


FIGURE 5 1D assessment of the results for (a) porosity, (b) clay content, (c) water saturation, (d) P-wave velocity, (e) S-wave velocity and (f) density at $X = 0.5$ km (center of the two-dimensional section). The true value is shown with the solid line, the estimated model is shown with the dashed line, and the dotted line presents the initial model.

accurate time-lapse image using this method due to the crosstalk between parameters. It is worth reminding that the crosstalk problem is more severe in time-lapse inversion because the magnitude of changes in reservoirs is comparable to generated artefacts. To improve the results, we follow another strategy. In this strategy, the rock physics properties of the baseline are estimated using Equation (17). Then, by assuming that porosity and clay content are not variable with time, the elastic properties of the monitor model are inverted to estimate the saturation. For this purpose, the estimated rock physics model of the baseline is used as the initial model to estimate the rock physics properties of the monitor model. Despite the inversion of the baseline model, we perform single-parameter inversion for estimating the rock physics properties of the monitor model during which only S_w is updated. This strategy leads to the time-lapse estimate presented in Figure 6d–f where a better time-lapse image of the saturation is obtained. This strategy is used hereafter in this study to compute the time-lapse rock physics properties using the DV parameterization. By using the PCS parameterization and considering time-independent porosity and clay content, direct TL-FWI is performed to only monitor the water saturation. The estimated time-lapse models of porosity, clay content and water saturation are presented in Figure 6g–i. Comparing Figure 6 to Figure 2j–l shows that the PCS parameterization can improve the accuracy of time-lapse studies for

monitoring the saturation of the fluids in the subsurface. The accuracy of the results is measured using root-mean-square error and direct monitoring of S_w using the PCS parameterization leads to a 37.3% higher accuracy in comparison to using the DV parameterization.

In addition to the rock physics properties, the PCS parameterization can be used to recover time-lapse images of the elastic properties. For this case, we use Equation (16) to obtain the baseline and monitor models in terms of porosity, clay content and water saturation. The results are then used for rock physics modelling (Equations 9–15) to obtain the elastic properties of the baseline and monitor models. While the DV parameterization leads to time-lapse images presented in Figure 7a–c, the PCS parameterization improves the time-lapse estimates (Figure 7d–f). The DV parameterization does not allow for recovering the changes appropriately. This can be explained by considering that 25% changes in the saturation (Figure 2l) are now spread out between three elastic properties, and it causes only 3%, 0.4% and 0.8% variation, respectively, in V_p , V_s and ρ (Figure 3j–l). Comparing the estimated time-lapse changes in Figure 7 shows that using the PCS parameterization, we can recover the elastic properties more accurately than using the DV parameterization. The time-lapse elastic properties estimated using the PCS parameterization are 53% more accurate than with the DV parameterization.

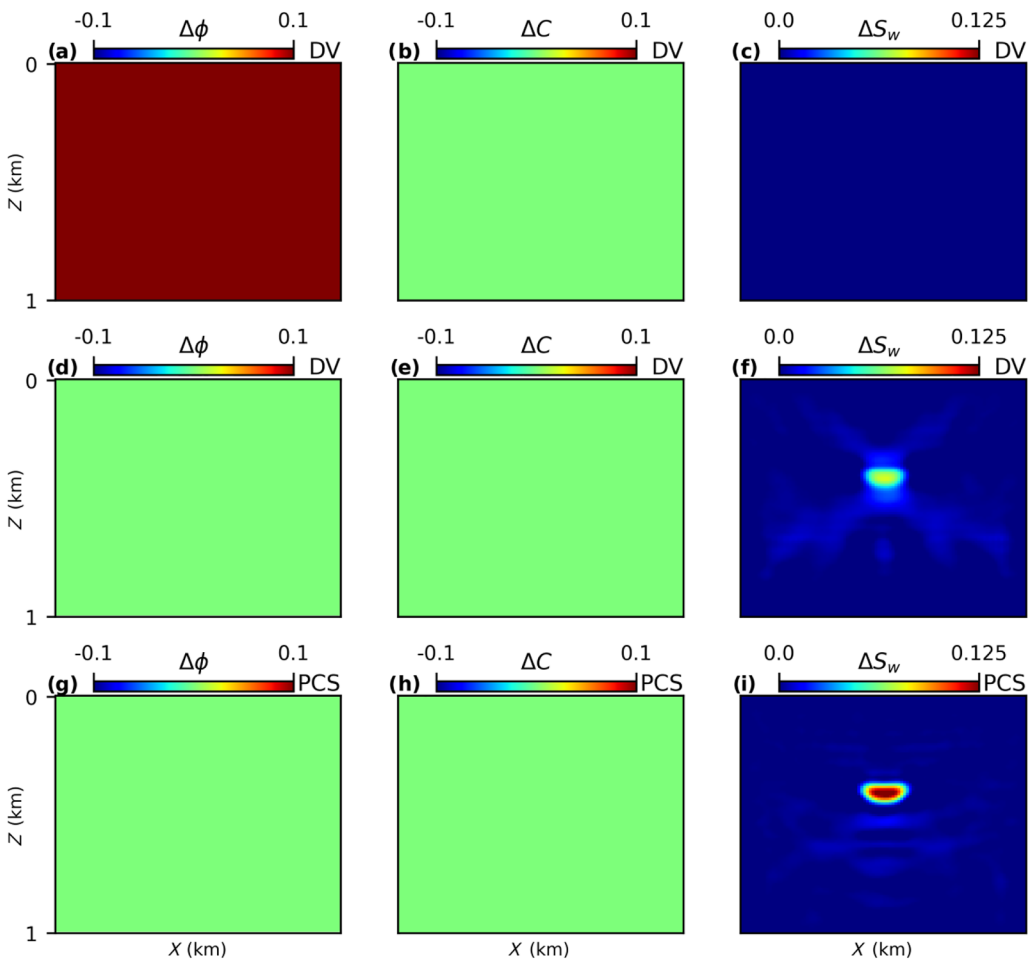


FIGURE 6 Estimated time-lapse model for ϕ , C and S_w with (a)–(c) the DV parameterization while all model parameters can vary with time, (d)–(f) the DV parameterization while S_w is the only time-dependent parameter, and (g)–(i) the PCS parameterization. DV, velocity–density. PCS, porosity–clay content–water saturation.

Figure 8a–c shows 1D profiles of the true and estimated changes in the rock physics properties along the dashed line in Figure 2l. The estimated time-lapse elastic properties from PCS and DV parameterizations are also compared in Figure 8d–f. This comparison shows that the results obtained using the DV parameterization (dotted lines) are far from accurate. For 1D analysis, the PCS parameterization leads to 43% higher accuracy (Figure 8a–c). For monitoring the elastic properties, the PCS parameterization yields 57% higher accuracy (Figure 8d–f).

Marmousi model

In this section, we aim at assessing the methodology using a more realistic model. For this purpose, a portion of the Marmousi model is chosen (Figure 9). The true baseline and monitor models are shown in Figure 9a–f. This model contains two sandstone reservoirs. The monitor model (Figure 9d–f) is created by reducing the water saturation in the reservoir indicated by line A₁ and increasing

the water saturation in the reservoir indicated by line A₂ (Figure 9l).

The elastic properties of this model are shown in Figure 10. Basically, the density of the saturated rock increases by replacing the hydrocarbon with water. Although the P-wave velocity has a reverse relationship with density, the hydrocarbon–water replacement increases the P-wave velocity due to the increase of the saturated bulk modulus. However, the fluid shear modulus is nil and S-wave velocity is decreased due to the increase in density. Figures 9j–l and 10j–l show the time-lapse changes in rock physics and elastic properties, respectively. The relative changes are shown in Figures 11a–c and 11d–f for the rock physics and elastic properties, respectively. In this case, the maximum changes in water saturation occur in the reservoir A₂, which shows a 40% change with respect to the baseline. This change leads to a maximum change of 6.2%, 2.31%, and 4.46% in elastic properties, V_P , V_S , and ρ , respectively. Hence, we can expect that changes can be better tracked using the PCS parameterization.

FWI of the baseline data is carried out using the PCS parameterization with values of, respectively, 5 and 8 for

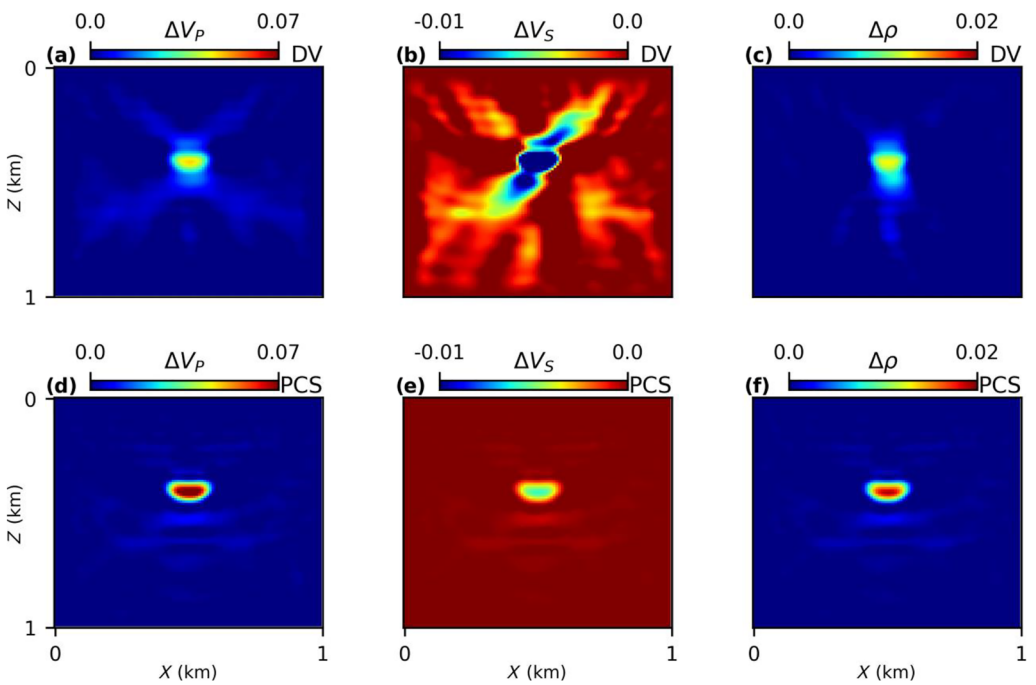


FIGURE 7 Estimated time-lapse model for V_p , V_s and ρ with (a)–(c) the DV parameterization and (d)–(f) the PCS parameterization (porosity-clay content-water saturation).

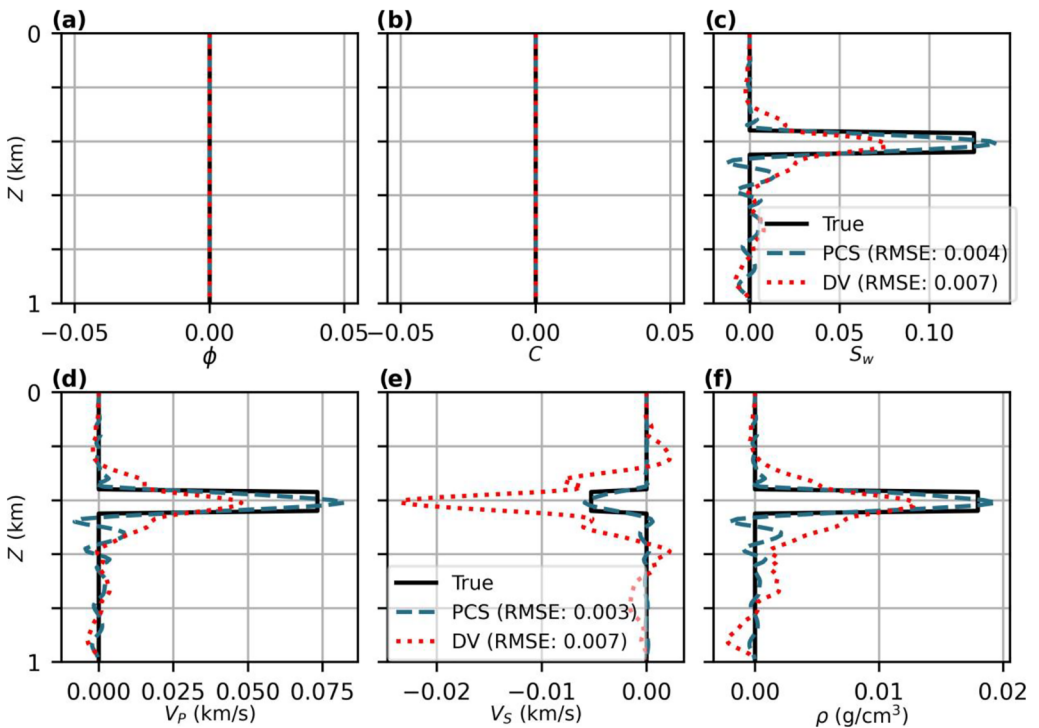


FIGURE 8 1D assessment of the time-lapse estimates for (a) porosity, (b) clay content, (c) water saturation, (d) P-wave velocity, (e) S-wave velocity and (f) density at $X = 0.5$ km. The true value is shown with the solid line, the estimated model with PCS parameterization is shown with the dashed line and the dotted line presents the estimated model with the DV parameterization. DV, density-velocity. PCS, porosity-clay content-water saturation.

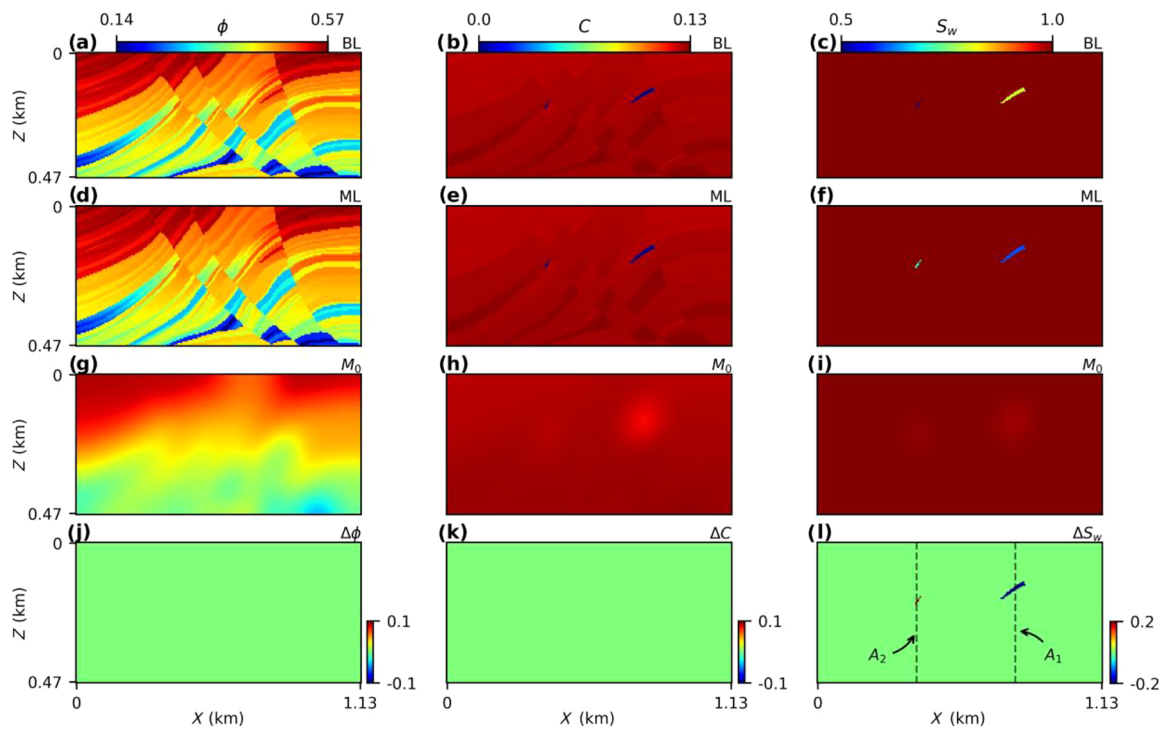


FIGURE 9 Rock-physics properties of the Marmousi model. (a)–(c) True baseline (BL), (d)–(f) true monitor (ML), and (g)–(i) initial models. (j)–(l) Time-lapse changes between porosity (a and d), clay content (b and e) and water saturation (c and f). Lines A_1 and A_2 are used for 1D studies in Figure 14.

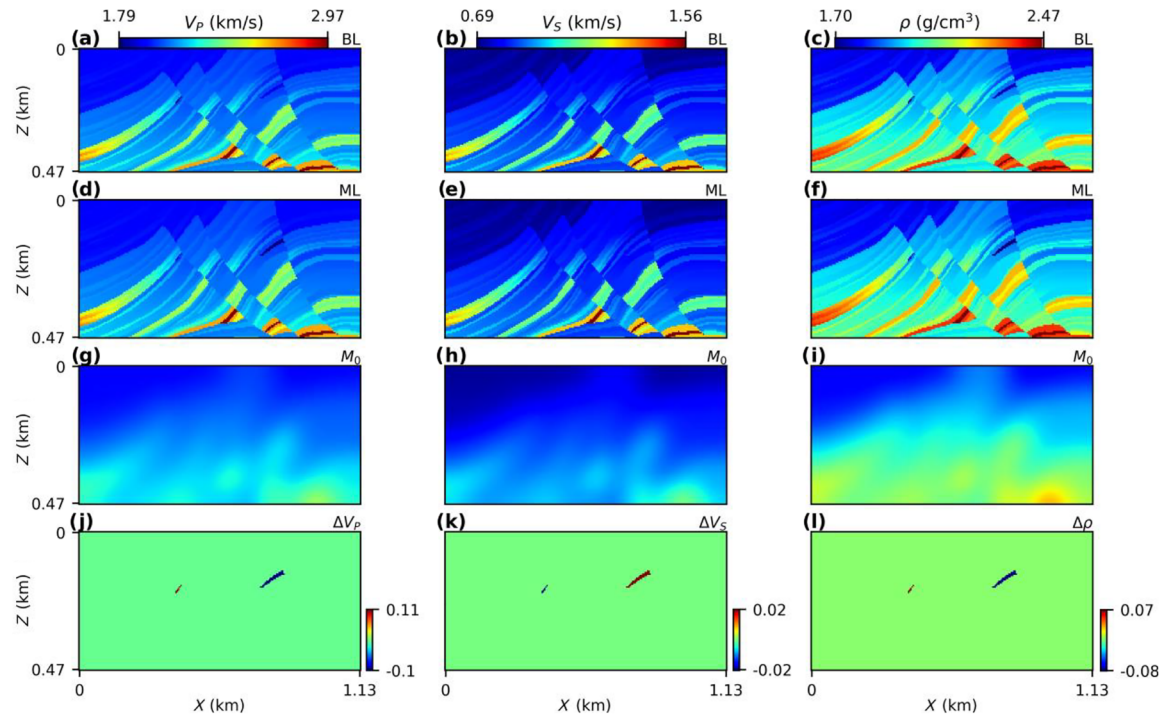


FIGURE 10 Elastic properties of the Marmousi model. (a)–(c) True baseline (BL), (d)–(f) true monitor (ML), and (g)–(i) initial models. (j)–(l) Time-lapse changes between V_P (a and d), V_S (b and e) and ρ (c and f).

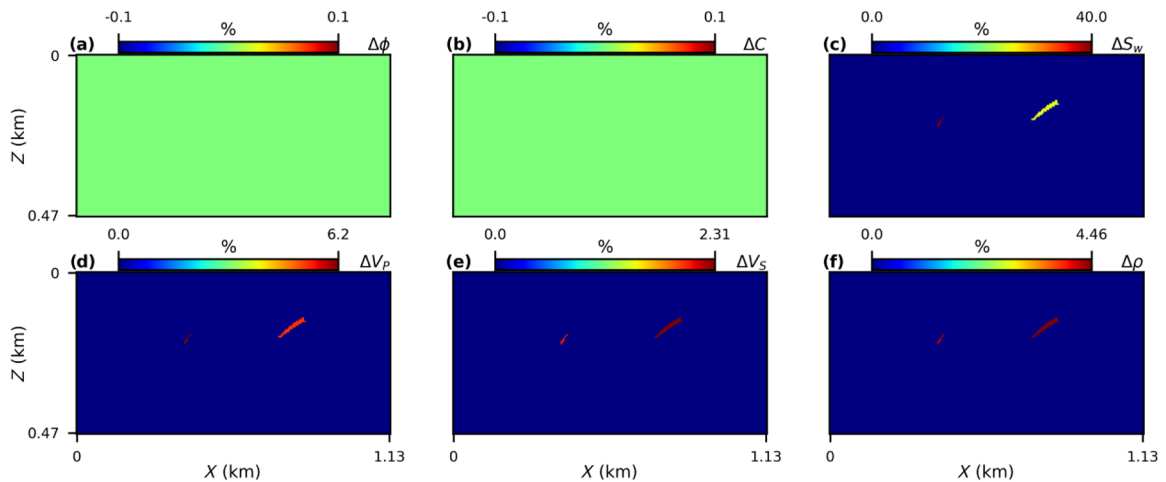


FIGURE 11 Absolute value of percent changes relative to the baseline in terms of studied (a)–(c) rock physics and (d)–(f) elastic properties.

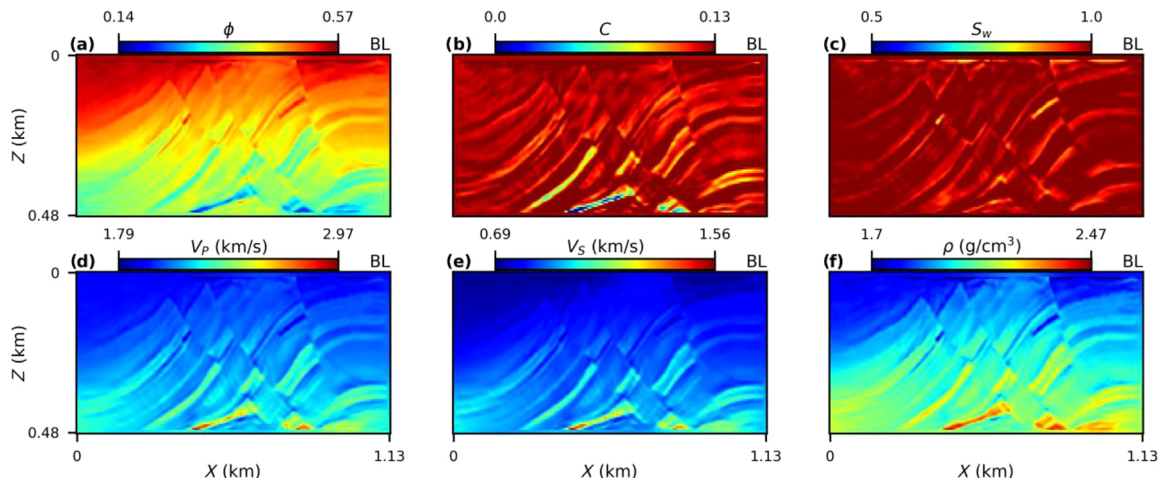


FIGURE 12 The estimated baseline models (BL) in terms of (a) porosity, (b) clay content, (c) water saturation, (d) P-wave velocity, (e) S-wave velocity and (f) density estimated using the PCS parameterization.

ξ and β , obtained from the layered model, studied in the previous section. The initial model for this inversion is presented in Figure 9g–i. The results of the inversion of the baseline are presented in Figure 12. As the receivers are located only on the surface for this model, it can be seen that the quality of the model update decreases towards the edges. Finally, the results of TL-FWI are shown in Figure 13. As shown in Figure 13a–c, the DV parameterization allows recovering changes in only reservoir A_1 . On the other hand, the time-lapse water saturation anomalies are detected in both reservoirs using the PCS parameterization, as shown in Figure 13d–f.

Figure 13g–l shows the changes in elastic properties. In this case, the PCS parameterization, shown in Figure 13j–l, yields significant improvement over the DV parameterization, shown in Figure 13g–i. This improvement leads to 11.7% higher accuracy by using the PCS parameterization. As can

be seen in Figure 13g, the changes in P-wave velocity are not recovered in reservoir A_2 . Although the time-lapse changes in S-wave velocity can be detected, the value in reservoir A_1 is overestimated (Figure 13h). Last but not least, the time-lapse anomalies of density are not detectable in Figure 13i. Despite inaccuracies in the estimated time-lapse elastic properties, Figure 13j–l shows that the PCS parameterization can lead to a better estimation of elastic properties.

Finally, a 1D assessment of the results is carried out along lines A_1 and A_2 , shown in Figure 9l. The 1D presentation of time-lapse changes (Figure 14) shows that TL-FWI with the DV parameterization is not able to recover the changes in the reservoirs appropriately while using the PCS parameterization can provide accurate time-lapse images of the model for both the elastic and rock physics properties. In this 1D analysis, the PCS parameterization leads to 24.51% higher accuracy for estimating the

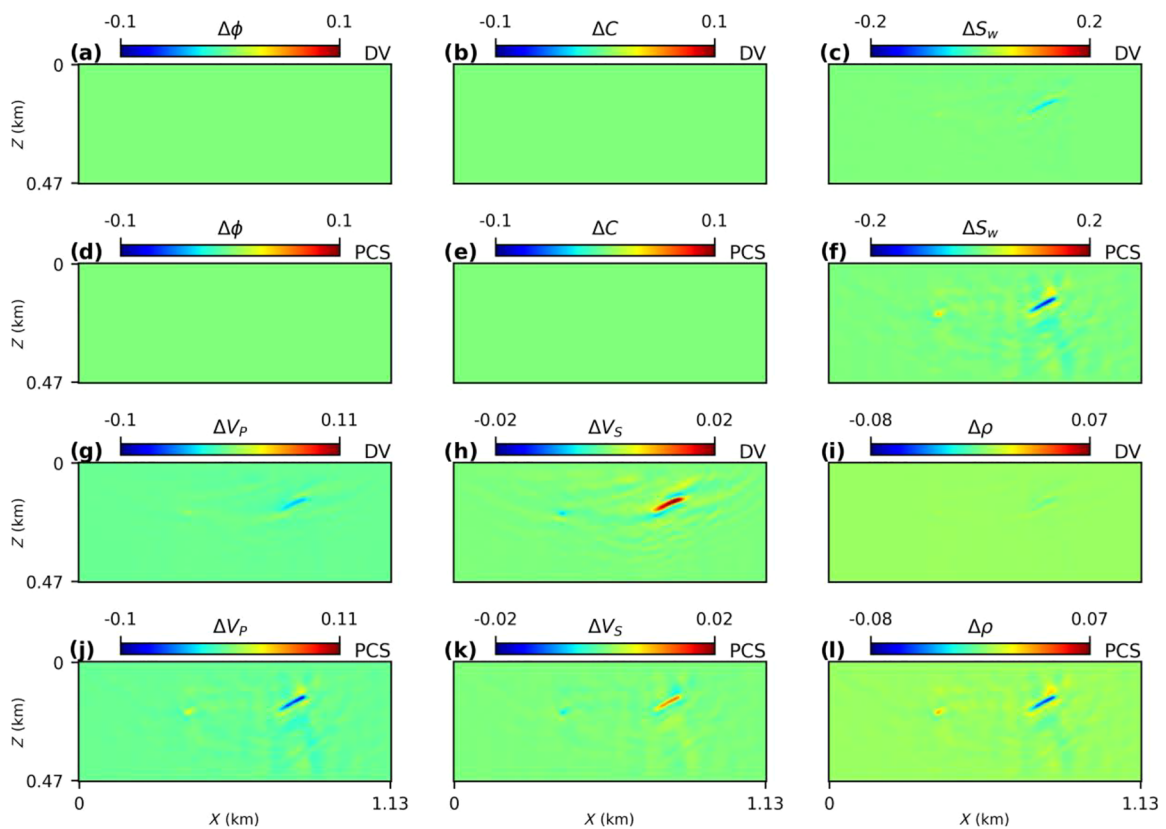


FIGURE 13 Estimated time-lapse model for ϕ , C and S_w with (a)–(c) the DV and (d)–(f) PCS parameterizations. The estimated time-lapse model for V_p , V_s and ρ with (g)–(i) the DV and (j)–(l) the PCS parameterizations (porosity-clay content-water saturation).

elastic properties and 19.57% for estimating the rock physics properties.

DISCUSSION

The potential of the PCS parameterization for estimating time-lapse changes in elastic and rock physics properties is shown in this study. The direct estimation of changes in rock physics properties provides more accurate results rather than the indirect estimation. However, the estimates presented in Figure 6 show clearly that an effective inversion strategy and optimization method can improve the accuracy of estimated changes using indirect inversion. As the computation time of the rock physics modelling is negligible, global inversion methods such as Monte Carlo methods might be a better choice for the second step of the inversion (Dupuy et al., 2016). However, the direct estimation of rock physics properties aids to avoid the challenges of picking an appropriate optimization method and parameters for the rock physics inversion.

The estimated time-lapse changes for the two presented synthetic models show that using the PCS parameterization

can also enhance the accuracy of monitoring the elastic properties (Figures 7 and 13). This is due to the fact that by using the PCS parameterization, the crosstalk between parameters of different vintages can be avoided. In this study, we assumed that the only variable parameter with time is fluid saturation. However, pore pressure is another important parameter that should be considered. Although the changes in the pore pressure can be negligible in some fields due to the properties such as high permeability (Dupuy et al., 2021), further studies should be conducted to analyse the efficiency of simultaneous monitoring of saturation and pore pressure.

In this work, we have assumed a simple rock physics model in which only saturation effects on elastic properties are modelled. In reality, this model will contain errors in describing the actual subsurface properties either from the calibration and subsurface assumptions or even the model itself. However, time-lapse studies are carried out in well-studied fields. The calibration of the rock physics model should not pose too much of a problem in this scenario. Besides, the geological information and well-log data of these fields can be employed to regularize the inversion problem and increase the accuracy of full-waveform inversion results.

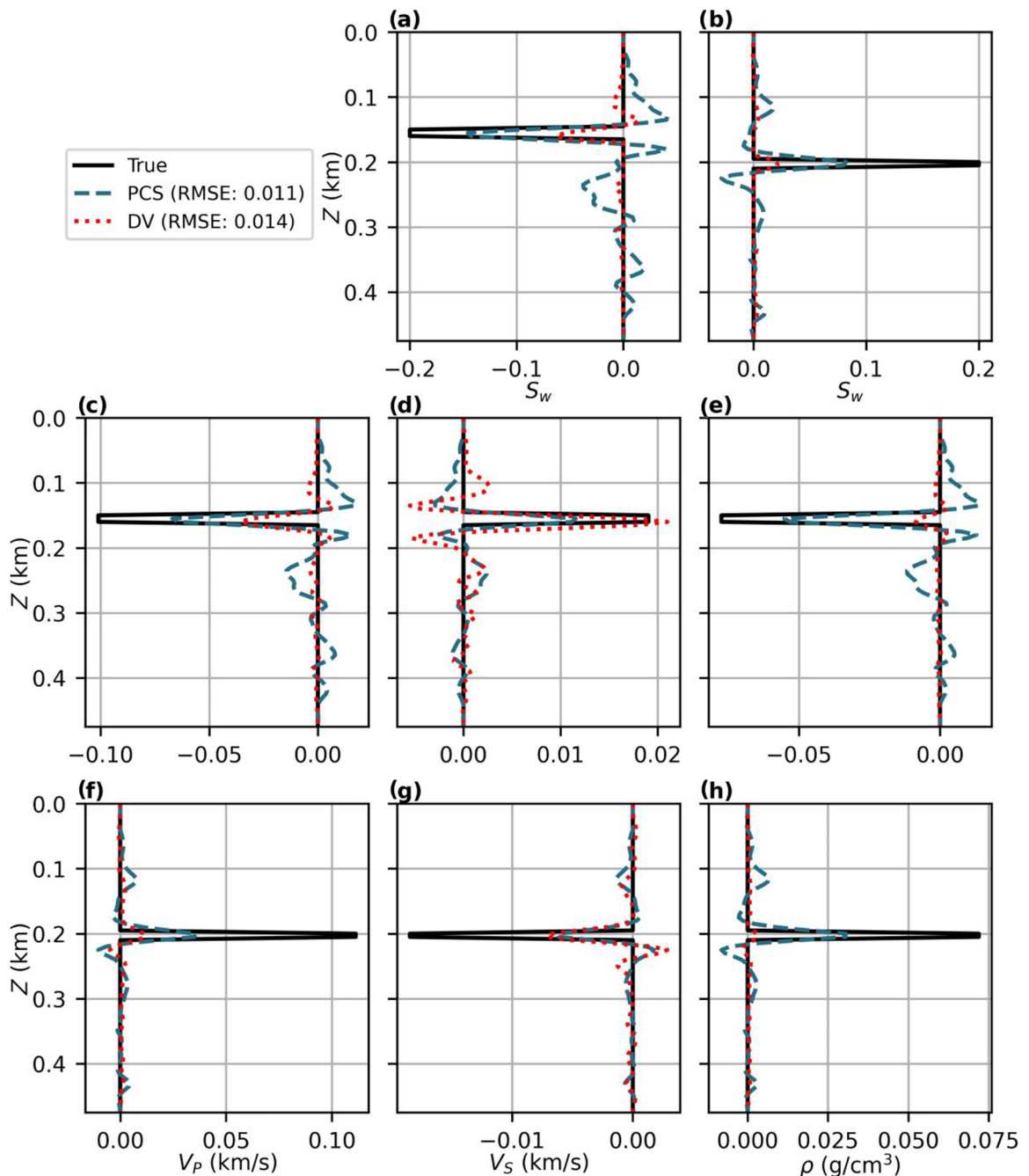


FIGURE 14 1D assessment of the time-lapse estimates for saturation along the line (a) A_1 and (b) A_2 . Time-lapse estimates for elastic properties along the line (c)–(e) A_1 and (f)–(h) A_2 . The true value is shown with the solid line, the estimated model with the PCS parameterization is shown with the dashed line and the dotted line presents the estimated model with the DV parameterization.

CONCLUSION

Time-lapse seismic data have been proven as an important source of information for reservoir monitoring. The full-waveform inversion is a powerful tool that relies on seismic data to recover the subsurface properties. However, this method generally suffers from crosstalk between parameters in multiparameter studies. This problem becomes more dramatic in time-lapse studies because the time-lapse changes

can be caused by any combination of different parameters in different vintages.

In this study, we formulated the time-lapse full waveform inversion in terms of porosity, clay content, and water saturation using Gassmann's equation, to assess its performance for reducing crosstalk and improve estimates of saturation changes. Using this formulation, we can rely on the assumption that water saturation is the only variable parameter that changes in time and, thereby, it is possible to avoid crosstalk

caused by the time-lapse study. We showed that the PCS parameterization improves the time-lapse estimate. By using Gassmann's equation and the new parameterization, it is also shown that the time-lapse estimate in elastic properties can be obtained indirectly with higher accuracy (11.7% higher accuracy in the case of the Marmousi model).

ACKNOWLEDGEMENTS

We would like to thank François Lavoué for valuable discussions on multiparameter full-waveform inversion. This project was supported by an NSERC Discovery Grant to BG (RGPIN-2017-06215). A. Mardan was also partially supported by the SEG/Landmark Scholarship.

DATA AVAILABILITY STATEMENT

Data associated with this research are available and can be obtained by contacting the corresponding author.

REFERENCES

- Anagaw, A.Y. & Sacchi, M.D. (2012) Edge-preserving seismic imaging using the total variation method. *Journal of Geophysics and Engineering*, 9(2), 138–146.
- Asnaashari, A., Brossier, R., Garambois, S., Audebert, F., Thore, P. & Virieux, J. (2013) Regularized seismic full waveform inversion with prior model information. *Geophysics*, 78(2), R25–R36.
- Asnaashari, A., Brossier, R., Garambois, S., Audebert, F., Thore, P. & Virieux, J. (2015) Time-lapse seismic imaging using regularized full-waveform inversion with a prior model: Which strategy? *Geophysical Prospecting*, 63(1), 78–98.
- Berenger, J.-P. (1994) A perfectly matched layer for the absorption of electromagnetic waves. *Journal of Computational Physics*, 114(2), 185–200.
- Berryman, J.G. (1995) Mixture theories for rock properties. In: *Rock physics and phase relations: A handbook of physical constants*. New York: Wiley, Vol. 3, 205–228.
- Buland, A. & Ouair, Y.E. (2006) Bayesian time-lapse inversion. *Geophysics*, 71(3), R43–R48.
- Bunks, C., Saleck, F.M., Zaleski, S. & Chavent, G. (1995) Multiscale seismic waveform inversion. *Geophysics*, 60(5), 1457–1473.
- Dupuy, B., Garambois, S., Asnaashari, A., Balhareth, H.M., Landrø, M., Stovas, A. & Virieux, J. (2016) Estimation of rock physics properties from seismic attributes - part 2: applications. *Geophysics*, 81(4), M55–M69.
- Dupuy, B., Garambois, S. & Virieux, J. (2016) Estimation of rock physics properties from seismic attributes - part 1: strategy and sensitivity analysis. *Geophysics*, 81(3), M35–M53.
- Dupuy, B., Romdhane, A., Eliasson, P. & Yan, H. (2021) Combined geophysical and rock physics workflow for quantitative CO₂ monitoring. *International Journal of Greenhouse Gas Control*, 106, 103217.
- Esser, E., Guasch, L., van Leeuwen, T., Aravkin, A.Y. & Herrmann, F.J. (2018) Total variation regularization strategies in full-waveform inversion. *SIAM Journal on Imaging Sciences*, 11(1), 376–406.
- Fabien-Ouellet, G., Gloaguen, E. & Giroux, B. (2017) Time domain viscoelastic full waveform inversion. *Geophysical Journal International*, 209(3), 1718–1734.
- Gassmann, F. (1951) Über die Elastizität poröser Medien. *Vierteljahrsschrift der Naturforschenden Gesellschaft in Zurich*, 96, 1–23.
- Hicks, E., Hoeber, H., Houbiers, M., Lescoffit, S.P., Ratcliffe, A. & Vinje, V. (2016) Time-lapse full-waveform inversion as a reservoir-monitoring tool - a North Sea case study. *The Leading Edge*, 35(10), 850–858.
- Hu, Q. & Innanen, K. (2021) Elastic full-waveform inversion with rock-physics constraints. In *First International Meeting for Applied Geoscience & Energy*. Houston, TX: Society of Exploration Geophysicists, pp. 662–666.
- Hu, Q., Keating, S., Innanen, K.A. & Chen, H. (2021) Direct updating of rock-physics properties using elastic full-waveform inversion. *Geophysics*, 86(3), MR117–MR132.
- Kamei, R. & Pratt, R.G. (2013) Inversion strategies for visco-acoustic waveform inversion. *Geophysical Journal International*, 194(2), 859–884.
- Keating, S. & Innanen, K.A. (2019) Parameter crosstalk and modeling errors in viscoacoustic seismic full-waveform inversion. *Geophysics*, 84(4), R641–R653.
- Landrø, M., Veire, H.H., Duffaut, K. & Najjar, N. (2003) Discrimination between pressure and fluid saturation changes from marine multicomponent time-lapse seismic data. *Geophysics*, 68(5), 1592–1599.
- Lang, X. & Grana, D. (2019) Rock physics modelling and inversion for saturation-pressure changes in time-lapse seismic studies. *Geophysical Prospecting*, 67(7), 1912–1928.
- Lavoué, F., Brossier, R., Métivier, L., Garambois, S. & Virieux, J. (2014) Two-dimensional permittivity and conductivity imaging by full waveform inversion of multioffset GPR data: a frequency-domain quasi-Newton approach. *Geophysical Journal International*, 197(1), 248–268.
- Lee, M.W. (2005) *Proposed moduli of dry rock and their application to predicting elastic velocities of sandstones*. Reston, VA: U.S. Department of the Interior, U.S. Geological Survey.
- Lescoffit, S.P., Houbiers, M., Henstock, C., Hicks, E., Nilsen, K.-M., Hoeber, H., Ratcliffe, A. & Vinje, V. (2016) Time-lapse full-waveform inversion applied to permanent reservoir monitoring data from Grane, a Norwegian North Sea field. In: *SEG Technical Program Expanded Abstracts 2016*. Houston, TX: Society of Exploration Geophysicists, pp. 1304–1308.
- Lumley, D.E. (2001) Time-lapse seismic reservoir monitoring. *Geophysics*, 66(1), 50–53.
- Ma, Y., Maharramov, M., Clapp, R. & Biondi, B. (2016) Multiparameter full-waveform inversion in the isotropic acoustic media with application to time-lapse seismic inverse problem. In: *SEG Technical Program Expanded Abstracts 2016*. Houston, TX: Society of Exploration Geophysicists, pp. 5557–5561.
- Maharramov, M., Biondi, B.L. & Meadows, M.A. (2016) Time-lapse inverse theory with applications. *Geophysics*, 81(6), R485–R501.
- Mallick, S. (2007) Amplitude-variation-with-offset, elastic-impedance, and wave-equation synthetics-a modeling study. *Geophysics*, 72(1), C1–C7.
- Mardan, A., Giroux, B. & Fabien-Ouellet, G. (2022a) Effects of non-repeatability on time-lapse full-waveform inversion. In *The Second EAGE Conference on Seismic Inversion*. Houten, the Netherlands: European Association of Geoscientists & Engineers, pp. 1–5.
- Mardan, A., Giroux, B. & Fabien-Ouellet, G. (2022b) Time-lapse full-waveform inversion for monitoring the fluid saturation. In: *The Second EAGE Conference on Seismic Inversion*. Houten, the Netherlands: European Association of Geoscientists & Engineers, pp. 1–5.
- Mardan, A., Giroux, B. & Fabien-Ouellet, G. (2022c) Time-lapse seismic full waveform inversion using improved cascaded method. In:



- The Second EAGE Conference on Seismic Inversion*. European Association of Geoscientists & Engineers, pp. 1–5.
- Mardan, A., Giroux, B. & Fabien-Ouellet, G. (2023a) PyFWI: A Python package for full-waveform inversion and reservoir monitoring. *SoftwareX* 22, 101384.
- Mardan, A., Giroux, B. & Fabien-Ouellet, G. (2023b) Weighted-average time-lapse seismic full-waveform inversion. *Geophysics*, 88(1), R25–R38.
- Mardan, A., Giroux, B., Fabien-Ouellet, G. & Saberi, M. (2022d) Direct monitoring of fluid saturation using time-lapse full-waveform inversion. In: *The Second International Meeting for Applied Geoscience & Energy Expanded Abstracts*. Houston, TX: Society of Exploration Geophysicists, pp. 3424–3428.
- Mavko, G., Mukerji, T. & Dvorkin, J. (2020) *The rock physics handbook*. New York: Cambridge University Press.
- Métivier, L., Brossier, R., Virieux, J. & Operto, S. (2013) Full waveform inversion and the truncated Newton method. *SIAM Journal on Scientific Computing*, 35(2), B401–B437.
- Naeini, E.Z., Kamath, N., Tsvankin, I. & Alkhalifah, T. (2017) Full waveform inversion for reservoir characterization-a synthetic study. In: *The 79th EAGE Conference and Exhibition 2017*, volume 2017. Houten, the Netherlands: European Association of Geoscientists & Engineers, pp. 1–5.
- Nocedal, J. & Wright, S.J. (2006) *Numerical optimization*. New York, NY: Springer.
- Operto, S., Gholami, Y., Prieux, V., Ribodetti, A., Brossier, R., Metivier, L., & Virieux, J. (2013) A guided tour of multiparameter full-waveform inversion with multicomponent data: from theory to practice. *The Leading Edge*, 32(9), 1040–1054.
- Pan, W., Innanen, K.A., Geng, Y. & Li, J. (2019) Interparameter trade-off quantification for isotropic-elastic full-waveform inversion with various model parameterizations. *Geophysics*, 84(2), R185–R206.
- Plessix, R., Michelet, S., Rynja, H., Kuehl, H., Perkins, C., de Maag, J. & Hatchell, P. (2010) Some 3D applications of full waveform inversion. In: *The 72nd EAGE Conference and Exhibition-Workshops and Fieldtrips*. Houten, the Netherlands: European Association of Geoscientists & Engineers.
- Pride, S. (2005) *Hydrogeophysics: Water science and technology library*. Berlin: Springer, pp. 253–284.
- Queißer, M. & Singh, S.C. (2013) Full waveform inversion in the time lapse mode applied to CO₂ storage at Sleipner. *Geophysical Prospecting*, 61(3), 537–555.
- Raknes, E.B., Weibull, W. & Arntsen, B. (2013) Time-lapse full waveform inversion: Synthetic and real data examples. In: *SEG Technical Program Expanded Abstracts 2013*. Houston, TX: Society of Exploration Geophysicists, pp. 944–948.
- Romdhane, A., Dupuy, B., Querendez, E. & Eliasson, P. (2022) Toward quantitative CO₂ monitoring at Sleipner, Norway. *Geophysical Monitoring for Geologic Carbon Storage*, 383–402.
- Tarantola, A. (1986) A strategy for nonlinear elastic inversion of seismic reflection data. *Geophysics*, 51(10), 1893–1903.
- Vedanti, N. & Sen, M.K. (2009) Seismic inversion tracks in situ combustion: a case study from Balol oil field, India. *Geophysics*, 74(4), B103–B112.
- Virieux, J., Asnaashari, A., Brossier, R., Métivier, L., Ribodetti, A. & Zhou, W. (2017) 6. *An introduction to full waveform inversion*. Houston, TX: Society of Exploration Geophysicists, pp. R1–1 to R1–40.
- Virieux, J. & Operto, S. (2009) An overview of full-waveform inversion in exploration geophysics. *Geophysics*, 74(6), WCC1–WCC26.
- Voigt, W. (1889) Ueber die beziehung zwischen den beiden elastizitätsconstanten isotroper körper. *Annalen der physik*, 274(12), 573–587.
- Watanabe, T., Shimizu, S., Asakawa, E. & Matsuoka, T. (2005) *Differential waveform tomography for time-lapse crosswell seismic data with application to gas hydrate production monitoring*. Houston, TX: Society of Exploration Geophysicists, pp. 2323–2326.
- Yan, H., Dupuy, B., Romdhane, A. & Arntsen, B. (2019) CO₂ saturation estimates at Sleipner (North Sea) from seismic tomography and rock physics inversion. *Geophysical Prospecting*, 67(4), 1055–1071. A special issue on Rock physics: from microstructure to seismic signatures/
- Yang, P., Brossier, R., Métivier, L., Virieux, J. & Zhou, W. (2018) A time-domain preconditioned truncated Newton approach to visco-acoustic multiparameter full waveform inversion. *SIAM Journal on Scientific Computing*, 40(4), B1101–B1130.
- Zhou, W. & Lumley, D. (2021) Central-difference time-lapse 4D seismic full-waveform inversion. *Geophysics*, 86(2), R161–R172.

How to cite this article: Mardan, A., Giroux, B., Fabien-Ouellet, G., & Saberi, M.R. (2023) Monitoring fluid saturation in reservoirs using time-lapse full-waveform inversion. *Geophysical Prospecting*, 1–18. <https://doi.org/10.1111/1365-2478.13363>

APPENDIX A: REGULARIZATION IN SEISMIC FULL-WAVEFORM INVERSION

By taking advantage of Tikhonov regularization, smoothness of the estimated model can be achieved (Asnaashari et al., 2013). This regularization can be presented as

$$\chi_1 = \lambda_1 (\mathbf{m}^T \mathbf{B}_x^T \mathbf{B}_x \mathbf{m} + \mathbf{m}^T \mathbf{B}_z^T \mathbf{B}_z \mathbf{m}), \quad (\text{A.1})$$

where \mathbf{B} and λ denote, respectively, the first-order spatial derivative operator and regularization hyperparameter. The subscripts x and z specify the direction.

Total variation regularization has also shown promising results in full-waveform inversion (FWI) to decrease artefacts and preserve the edges and the discontinuities (Anagaw & Sacchi, 2012; Esser et al., 2018). This regularization can be achieved by using

$$\chi_2 = \lambda_2 \sqrt{(\mathbf{B}_x \mathbf{m})^2 + (\mathbf{B}_z \mathbf{m})^2} \|_1. \quad (\text{A.2})$$

Also, Asnaashari et al. (2013) state that where nonseismic information exists, it should be used as prior information for FWI inversion. Hence, they proposed regularizing the cost function using the prior information (\mathbf{m}_p) as

$$\chi_3 = \lambda_3 \|\mathbf{W}_m (\mathbf{m} - \mathbf{m}_p)\|_2^2, \quad (\text{A.3})$$

where \mathbf{W}_m is a weighting operator in the model space.

Finally, in the case of multiparameter FWI, if information about the relationship between different parameters exists, then regularization can be considered to force the optimization algorithm to follow (Hu & Innanen, 2021),

$$\chi_4 = \lambda_4 \|\mathbf{m}_1 - f(\mathbf{m}_2)\|_2^2, \quad (\text{A.4})$$

where f is a function to estimate \mathbf{m}_1 from \mathbf{m}_2 .

APPENDIX B: GRADIENT OF THE COST FUNCTION

In Equation (13), we showed how to calculate the elastic properties of the porous medium using K , G , and ρ . To perform full-waveform inversion (FWI) with PCS parameterization, it is required to estimate the gradient of these parameters in terms of PCS parameterization. The gradient of K , G , and ρ with respect to ϕ can be obtained as

$$\begin{aligned} \frac{\partial K}{\partial \phi} &= \frac{K_D + \phi \frac{\partial K_D}{\partial \phi} - \frac{K_f}{K_s} \left(K_D + (1 + \phi) \frac{\partial K_D}{\partial \phi} \right)}{\phi(1 + \Delta)} \\ &\quad \frac{\left[\phi K_D + \left(1 - \frac{(1 + \phi) K_D}{K_s} \right) K_f \right] \left(1 + \Delta + \phi \frac{\partial \Delta}{\partial \phi} \right)}{\phi^2(1 + \Delta)^2}, \end{aligned} \quad (\text{B.1})$$

$$\frac{\partial G}{\partial \phi} = \frac{\partial G_D}{\partial \phi},$$

$$\frac{\partial \rho}{\partial \phi} = \rho_f - \rho_s,$$

where

$$\begin{aligned} \frac{\partial K_D}{\partial \phi} &= -K_s \frac{1 + cs}{(1 + cs\phi)^2}, \\ \frac{\partial \Delta}{\partial \phi} &= -\frac{K_f}{K_s \phi^2} \left(1 - \frac{1}{1 + cs\phi} \right) + \frac{K_f(1 - \phi)}{K_s \phi} \frac{cs}{(1 + cs\phi)^2}, \\ \frac{\partial G_D}{\partial \phi} &= -G_s \frac{1 + \frac{3}{2}cs}{(1 + \frac{3}{2}cs\phi)^2}. \end{aligned} \quad (\text{B.2})$$

With respect to C , we have

$$\begin{aligned} \frac{\partial K}{\partial C} &= \frac{\phi \frac{\partial K_D}{\partial C} + \frac{K_f(1 + \phi)}{K_s^2} \left(\frac{\partial K_s}{\partial C} K_D - \frac{\partial K_D}{\partial C} K_s \right)}{\phi(1 + \Delta)} - \\ &\quad \frac{\left[\phi K_D + \left(1 - \frac{(1 + \phi) K_D}{K_s} \right) K_f \right] \phi \frac{\partial \Delta}{\partial C}}{\phi^2(1 + \Delta)^2}, \end{aligned} \quad (\text{B.3})$$

$$\frac{\partial G}{\partial C} = \frac{\partial G_D}{\partial C},$$

$$\frac{\partial \rho}{\partial C} = (1 - \phi) \frac{\partial \rho_s}{\partial C},$$

where

$$\begin{aligned} \frac{\partial \Delta}{\partial C} &= \frac{(\phi - 1) K_f}{\phi K_s^2} \left(1 - \frac{1}{1 + cs\phi} \right) \frac{\partial K_s}{\partial C}, \\ \frac{\partial K_s}{\partial C} &= K_c - K_q, & \frac{\partial G_s}{\partial C} &= G_c - G_q, \\ \frac{\partial K_D}{\partial C} &= \frac{1 - \phi}{1 + cs\phi} \frac{\partial K_s}{\partial C}, & \frac{\partial G_D}{\partial C} &= \frac{1 - \phi}{1 + \frac{3}{2}cs\phi} \frac{\partial G_s}{\partial C}, \\ \frac{\partial \rho_s}{\partial C} &= (\rho_c - \rho_q). \end{aligned} \quad (\text{B.4})$$

Finally, with respect to S_w , we have

$$\begin{aligned} \frac{\partial K}{\partial S_w} &= \frac{\left(1 - \frac{(1 + \phi) K_D}{K_s} \right) \frac{\partial K_f}{\partial S_w}}{\phi(1 + \Delta)} - \\ &\quad \frac{\left[\phi K_D + \left(1 - \frac{(1 + \phi) K_D}{K_s} \right) K_f \right] \phi \frac{\partial \Delta}{\partial S_w}}{\phi^2(1 + \Delta)^2}, \\ \frac{\partial G}{\partial S_w} &= 0, \\ \frac{\partial \rho}{\partial S_w} &= \phi(\rho_w - \rho_h), \end{aligned} \quad (\text{B.5})$$

where

$$\begin{aligned} \frac{\partial K_f}{\partial S_w} &= K_w - K_h, \\ \frac{\partial \Delta}{\partial S_w} &= \frac{\Delta}{K_f} \frac{\partial K_f}{\partial S_w}. \end{aligned} \quad (\text{B.6})$$

Gathering the previous terms, the gradient of the cost function with respect to model parameters in the PCS parameterization can be calculated as

$$\begin{bmatrix} \frac{\partial \chi}{\partial \phi} \\ \frac{\partial \chi}{\partial C} \\ \frac{\partial \chi}{\partial S_w} \end{bmatrix} = \begin{bmatrix} \frac{\partial V_p}{\partial \phi} & \frac{\partial V_s}{\partial \phi} & \frac{\partial \rho}{\partial \phi} \\ \frac{\partial V_p}{\partial C} & \frac{\partial V_s}{\partial C} & \frac{\partial \rho}{\partial C} \\ \frac{\partial V_p}{\partial S_w} & \frac{\partial V_s}{\partial S_w} & \frac{\partial \rho}{\partial S_w} \end{bmatrix} \begin{bmatrix} \frac{\partial \chi}{\partial V_p} \\ \frac{\partial \chi}{\partial V_s} \\ \frac{\partial \chi}{\partial \rho} \end{bmatrix}. \quad (\text{B.7})$$